

## Direct identification of the synergism between methyl radicals and atomic hydrogen during growth of amorphous hydrogenated carbon films

A. von Keudell,<sup>a)</sup> T. Schwarz-Selinger, M. Meier, and W. Jacob  
Max-Planck-Institut für Plasmaphysik, EURATOM Association, Boltzmannstrasse 2,  
85748 Garching, Germany

(Received 12 October 1999; accepted for publication 8 December 1999)

The simultaneous interaction of methyl radicals ( $\text{CH}_3$ ) and atomic hydrogen (H) with the surface of amorphous hydrogenated carbon ( $a\text{-C:H}$ ) film is investigated. Two identical quantified beam sources for H and  $\text{CH}_3$  are used. The growth and/or erosion during the simultaneous interaction of the two beams with an amorphous hydrogenated carbon film is monitored by using *in situ* real-time ellipsometry at a substrate temperature of 320 K. Interaction with the  $\text{CH}_3$  beam alone causes slow growth, corresponding to a sticking coefficient for  $\text{CH}_3$  of  $\sim 3 \times 10^{-5}$ . Simultaneous interaction of the atomic hydrogen beam and the  $\text{CH}_3$  radical beam yields a sticking coefficient for  $\text{CH}_3$  of  $3 \times 10^{-3}$ , which is two orders of magnitude larger than for  $\text{CH}_3$  alone. From a microscopic modeling of this synergistic growth, the reaction probability for  $\text{CH}_3$  adsorbing at an adsorption site, which is created by atomic hydrogen at the surface, is derived to be 0.14. © 2000 American Institute of Physics. [S0003-6951(00)01306-1]

The interaction of methyl radicals ( $\text{CH}_3$ ) and atomic hydrogen (H) with the surface of carbon or hydrocarbon films ( $a\text{-C:H}$ ) plays an important role in the understanding of the growth of these films from low-temperature plasmas.<sup>1,2</sup> For the deposition of amorphous hydrogenated carbon films from glow discharges using a hydrocarbon precursor gas such as methane, atomic hydrogen and  $\text{CH}_3$  radicals represent the dominant contributions of the impinging radical flux, as was shown by mass spectrometry.<sup>3,4</sup> In diamond deposition from discharges using a mixture of a few percent methane in hydrogen, the microscopic growth mechanism is believed to be the adsorption of  $\text{CH}_3$  at free surface sites, which are created via the abstraction of surface-bonded hydrogen by incoming atomic hydrogen.<sup>5-8</sup> Albeit this dominant role for the simultaneous interaction of H and  $\text{CH}_3$  with the growing film surface, only few experimental data on reaction probabilities are known. Only the cross sections for the interaction of atomic hydrogen with  $a\text{-C:H}$  films have been measured by Küppers,<sup>9</sup> and yielded  $0.05 \text{ \AA}^2$  for the abstraction of surface bonded hydrogen by H and  $1.3 \text{ \AA}^2$  for H adsorption at a dangling bond.

In this letter, we report on experiments using two quantified radical sources for methyl radicals and atomic hydrogen in order to measure reaction probabilities. The simultaneous interaction of these two radical beams with the surface of an amorphous hydrogenated carbon film is investigated using *in situ* real-time ellipsometry to monitor the growth and/or etch rate.

Methyl radicals or atomic hydrogen atoms are produced via thermal dissociation of a precursor gas in a heated tungsten capillary. The inner diameter of the capillary is 1 mm. Our implementation of such type of radical source is similar to the design developed by Horn *et al.*<sup>10</sup> The tip of the capillary is resistively heated and its temperature is measured by pyrometry. In order to protect the samples from the thermal

load due to the radiation of the hot tungsten capillary a water cooled copper shield is used. Two identical radical sources for  $\text{CH}_3$  and atomic hydrogen are implemented. The radical source for atomic hydrogen is operated at a capillary temperature of 2100 K and a gas flow of 0.1 sccm  $\text{H}_2$  through the capillary, controlled by a mass flow controller. The emitted absolute flux of atomic hydrogen as well as the angular distribution is determined in a separate experimental setup by using ionization threshold mass spectrometry (ITMS), yielding a flux of  $1 \times 10^{16} \text{ cm}^{-2} \text{ s}^{-1}$  at the substrate surface. Details on the quantification and on the implementation of this source for atomic hydrogen are presented elsewhere.<sup>11</sup> The radical source for  $\text{CH}_3$  is operated at a capillary temperature of 1150 K. At this temperature, the precursor gas azomethane  $\text{N}_2(\text{CH}_3)_2$  decomposes efficiently into  $\text{N}_2$  and  $2\text{CH}_3$  and produces a flux of  $\text{CH}_3$  radicals of  $1 \times 10^{15} \text{ cm}^{-2} \text{ s}^{-1}$  at the substrate surface which was quantified by mass spectrometry. The precursor gas azomethane is produced in a small oven via the thermal release from an azomethane- $\text{CuCl}_2$  complex at an oven temperature of about 320 K.<sup>12</sup> The heating power is feedback controlled by a baratron gauge, which measures the pressure in the gas line of the  $\text{CH}_3$  radical source. This gas pressure is kept constant at 1.5 mbar, thus maintaining a constant  $\text{CH}_3$  radical flux. Details on the implementation and quantification of the  $\text{CH}_3$  radical source will be presented elsewhere.<sup>13</sup> The two radical sources are mounted on an UHV system with a distance of 46 mm between sample and capillary tip. The base pressure is at  $10^{-9}$  mbar. A schematic sketch of the experimental setup is shown in Fig. 1. With both sources operating, the chamber pressure is  $1.5 \times 10^{-5}$  mbar.

The surface of an  $a\text{-C:H}$  film with a thickness of  $\sim 32$  nm is used as the sample. The film is deposited onto a single crystalline silicon wafer in a separate setup applying a rf discharge in methane at a pressure of 2 Pa and a dc self-bias of  $-300$  V. The films have a H/C ratio of 0.41 and a density of about  $1.9 \text{ g/cm}^3$ , determined by ion-beam analysis proton

<sup>a)</sup>Corresponding author; electronic mail: von\_Keudell@ipp.mpg.de

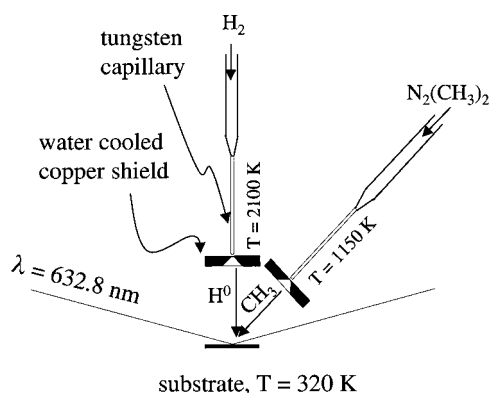


FIG. 1. Schematic sketch of the experimental setup.

enhanced scattering (PES) and elastic recoil detection (ERD).<sup>14,15</sup> The samples are transferred into the ultrahigh vacuum (UHV) system via a loadlock. The substrate temperature is measured by thermocouples. The heating of the capillaries of both radical sources is started 20 h prior to the beginning of the exposure of the sample to the H and CH<sub>3</sub> beam in order to achieve thermal equilibrium of the whole setup. Without additional external heating of the substrate under these conditions, a substrate temperature of 320 K is reached. The beams are switched on and off by switching the gas flow through the capillaries on and off.

Growth and erosion of the hydrocarbon films during interaction with the CH<sub>3</sub> and H beams is monitored using a rotating analyzer ellipsometer.<sup>16</sup> The angle of incidence is 74.85° and the optical properties are measured at a wavelength of 632.8 nm. For each data point 50 revolutions of the analyzer are averaged, yielding a time separation of the data points of 3.38 s.

Figure 2 shows the change of the ellipsometric angles during the interaction of the CH<sub>3</sub> and H beams with the hard *a*-C:H film. At the beginning of the experiment, only the H beam is switched on, and the ellipsometric angles change

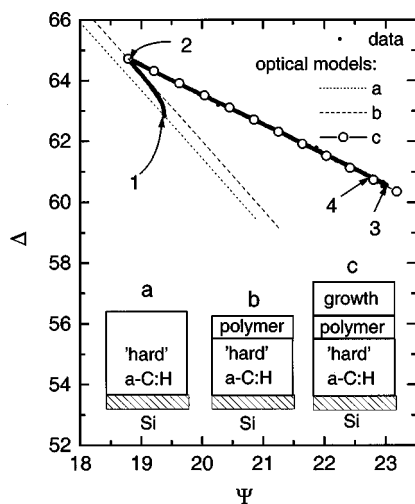


FIG. 2. Change of the ellipsometric angles during exposure of a hard *a*-C:H film to the CH<sub>3</sub> and H beams (closed circles). (a) Optical model for the hard *a*-C:H film with refractive index  $n = 2.1 - i0.1$  and variable film thickness. (b) Optical model for the hard *a*-C:H film with variable film thickness and a 1 nm top layer with refractive index  $n = 1.48 - i0$ . (c) Optical model for a polymer-like film with refractive index  $n = 1.55 - i0$  and variable film thickness on top of a 29.98 nm hard *a*-C:H film with a 1 nm interface with  $n = 1.48 - i0$ . The numbers indicate switching on and off of the radical beams.

from point 1 to point 2, as shown in Fig. 2. Then the CH<sub>3</sub> beam is switched on additionally and the ellipsometric angles change from point 2 to point 3. While the CH<sub>3</sub> beam is on, the H beam is switched on and off and, in addition, the H flux is varied by changing the H<sub>2</sub> gas flow. The ellipsometric angles remain on the line between point 2 and point 3 during variation of the H flux, which indicates that only the growth rate changes and not the optical film properties. At point 3 the CH<sub>3</sub> beam is switched off and the ellipsometric angles change from point 3 to point 4, indicating a slight etching of the film.

The ellipsometric data are fitted with optical models as illustrated in Figs. 2(a)–(c).

The optical model in Fig. 2(a) corresponds to an *a*-C:H film with a complex refractive index  $n = 2.1 - i0.1$  and a variable film thickness (dotted line in Fig. 2). At point 1, the ellipsometric angles correspond to a film thickness of 32.48 nm for the initial film prior to exposure to the radical beams.

The optical model in Fig. 2(b) corresponds to an *a*-C:H film ( $n = 2.1 - i0.1$ ) with variable film thickness and a top layer of 1 nm thickness with refractive index  $n = 1.48 - i0$  (dashed line in Fig. 2). After switching on the H beam, the ellipsometric angles change from point 1 to point 2, which can be modeled by assuming that the optical properties in a 1 nm top layer change gradually from  $n = 2.1 - i0.1$  to  $1.48 - i0$  and that the total film thickness decreases by 1.5 nm. This is consistent with the basic surface mechanisms for atomic hydrogen at the surface of an *a*-C:H film known from literature:<sup>9,17</sup> atomic hydrogen hydrogenates  $sp^2$  carbon-carbon double bonds at the hydrocarbon film surface and forms  $sp^3$  carbon groups. Since the extinction coefficient at 632.8 nm is due to the presence of  $sp^2$  groups in the initial *a*-C:H film, the transformation of  $sp^2$  groups into  $sp^3$  groups leads to the decrease of the extinction coefficient in the top layer from 0.1 to 0. In addition, the interaction of atomic hydrogen with the *a*-C:H film leads to a structural change towards a hydrogen-rich polymer-like film with a lower film density, indicated by the decrease of the refractive index from 2.1 to 1.48. This occurs only in a top layer of about 1 nm, corresponding to the maximum range of atomic hydrogen in *a*-C:H. Finally, at elevated substrate temperature, atomic hydrogen leads to slight etching of the film, indicated by the decrease in total film thickness.

The optical model in Fig. 2(c) corresponds to an *a*-C:H layer ( $n = 2.1 - i0.1$ ) with a thickness of 29.98 nm, an interface layer ( $n = 1.48 - i0$ ) with a thickness of 1 nm, and a growing film with refractive index  $n = 1.55 - i0$  and variable film thickness (open circles in Fig. 2; the distance between two model points corresponds to a 1 nm change of the film thickness). At point 2, the CH<sub>3</sub> beam is switched on and growth of an *a*-C:H film with a film thickness of 10.5 nm from point 2 to point 3 is observed. The refractive index indicates the formation of a hydrogen-rich polymer-like film. The density and the hydrogen to carbon ratio of this hydrogen-rich polymer-like film can be quantified based on the strong correlation among the material properties:<sup>18</sup> a refractive index of  $n = 1.55 - i0$  of the top layer corresponds to a density of  $1 \text{ g cm}^{-3}$  and a H/C ratio of 0.93. Based on the optical modeling, the change in the ellipsometric data is transferred into a variation of the film thickness. Using the

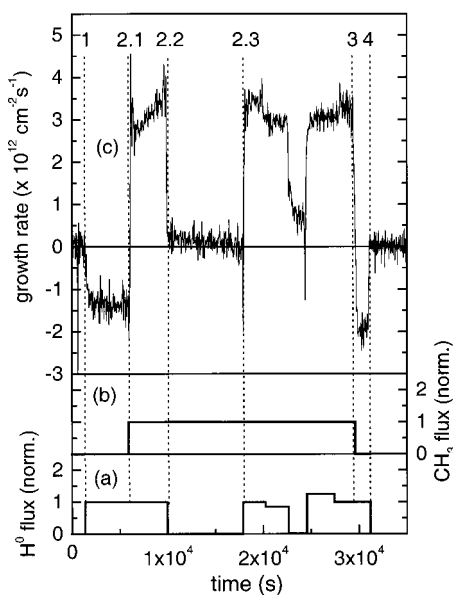


FIG. 3. (a) Variation of the impinging flux of H radicals normalized with  $10^{16} \text{ cm}^{-2} \text{ s}^{-1}$ . (b) Variation of the impinging flux of  $\text{CH}_3$  radicals normalized with  $2.5 \times 10^{15} \text{ cm}^{-2} \text{ s}^{-1}$ . (c) Variation of the growth and/or etch rate during exposure of the  $\alpha\text{-C:H}$  film to the  $\text{CH}_3$  and H beams. The numbers indicate changes in the beam parameters during the experiment.

density of  $1 \text{ g cm}^{-3}$ , the change in the film thickness is transferred into growth/etch rate expressed in incorporated/released carbon atoms per area and second respectively.

Figures 3(a) and 3(b) show the variation of the H and the  $\text{CH}_3$  flux of the impinging radical beams. Figure 3(c) shows the corresponding variation of the growth and etch rate, respectively, determined from the change in the ellipsometric angles and the optical model, shown in Fig. 2. At the beginning of the experiment (from point 1 to point 2.1 in Fig. 3), the hydrogenation of the hard carbon film is indicated by the slow increase and the subsequent saturation of the etch rate. At point 2.1, the  $\text{CH}_3$  radical beam is switched on and etching changes into growth at an almost constant rate. The sticking coefficient under the “hydrogen beam on” condition is  $3 \times 10^{-3}$ . At point 2.2 the atomic hydrogen beam is switched off, and the growth rate drops significantly, although the  $\text{CH}_3$  radical flux remains constant. The sticking coefficient under “H beam off” conditions is  $1.3 \times 10^{-5}$ . This proves that  $\text{CH}_3$  adsorption is strongly enhanced by a simultaneous flux of atomic hydrogen. This synergistic effect leads to a dramatic change in the sticking coefficient by  $10^2$ . At point 2.3, the atomic hydrogen beam is switched on again and growth proceeds at the same rate as before (between 2.1 and 2.2). Between point 2.3 and point 3 the atomic hydrogen flux is varied, and the growth rate follows the variation of the atomic hydrogen flux. At point 3 the  $\text{CH}_3$  beam is switched off again and the growth changes instantaneously into etching. Finally, at point 4, the hydrogen flux is stopped.

The growth synergism between  $\text{CH}_3$  and H can be explained as follows. It is widely assumed in the literature that  $\text{CH}_3$  adsorbs at dangling bonds which are created via the

abstraction of surface bonded hydrogen due to incoming atomic hydrogen.<sup>5–8</sup> These dangling bonds serve as adsorption sites for incoming  $\text{CH}_3$  radicals. The total number of surface sites can be estimated from the density of  $1 \text{ g cm}^{-3}$  for the polymer-like  $\alpha\text{-C:H}$  film, yielding  $1.2 \times 10^{15} \text{ cm}^{-2}$ . With this number, the cross sections for the surface reactions measured by Küppers<sup>9</sup> can be converted into reaction probabilities per surface site: the cross section of  $0.05 \text{ \AA}^2$  for the abstraction of surface bonded hydrogen by H gives  $p_{\text{abstraction}} = 0.006$  and the cross section of  $1.3 \text{ \AA}^2$  for H adsorption at a dangling bond gives  $p_{\text{recombination}} = 0.157$ . The steady state growth during the simultaneous interaction of  $\text{CH}_3$  and H with the  $\alpha\text{-C:H}$  film is modeled by a simple balance equation for the number of free sites at the surface: (i) dangling bonds are created via hydrogen abstraction by H with probability  $p_{\text{abstraction}}$ ; (ii) these dangling bonds can recombine with H with probability  $p_{\text{recombination}}$ , or (iii) they can recombine with  $\text{CH}_3$  with probability  $p_{\text{adsorption}}$  leading to film growth. It is assumed that synergistic growth occurs at the physical surface and that impinging species, which do not react, are reflected. Based on the steady state solution for this balance equation, including the known reaction probabilities for H, the incoming fluxes of  $\text{CH}_3$  and H radicals and the measurement of the growth rate, one obtains for the reaction probability for  $\text{CH}_3$  adsorption at a dangling bond  $p_{\text{adsorption}} = 0.14$ . A detailed analysis of this reaction scheme and the investigation of the dependence of this synergistic growth mechanism on the incoming radical fluxes will be subject of future experiments.

Thanks are due to C. Linsmeier for his assistance with the preparation of azomethane.

<sup>1</sup> W. Jacob, *Thin Solid Films* **326**, 1 (1998).

<sup>2</sup> W. Möller, W. Fukarek, K. Lange, A. von Keudell, and W. Jacob, *Jpn. J. Appl. Phys., Part 1* **34**, 2163 (1995).

<sup>3</sup> P. Pecher and W. Jacob, *Appl. Phys. Lett.* **73**, 31 (1998).

<sup>4</sup> H. Sugai, H. Kojima, A. Ishida, and H. Toyoda, *Appl. Phys. Lett.* **56**, 2616 (1990).

<sup>5</sup> S. J. Harris, *Appl. Phys. Lett.* **56**, 2298 (1990).

<sup>6</sup> M. Frenklach, S. Sokolov, and B. Weiner, *Nature (London)* **372**, 534 (1994).

<sup>7</sup> S. J. Harris and D. G. Goodwin, *J. Phys. Chem.* **97**, 23 (1993).

<sup>8</sup> B. J. Garrison, E. J. Dawnkaski, D. Srivastava, and D. W. Brenner, *Science* **255**, 835 (1992).

<sup>9</sup> J. Küppers, *Surf. Sci. Rep.* **22**, 249 (1995).

<sup>10</sup> A. Horn, T. Kammler, and M. Kappel, German Patent No. DE 197 57 851 C1 filed (1997).

<sup>11</sup> T. Schwarz-Selinger, A. von Keudell, and W. Jacob (unpublished).

<sup>12</sup> M. Remmler, B. Ondruschka, and G. Zimmermann, *J. Prakt. Chem.* **327**, 868 (1985).

<sup>13</sup> T. Schwarz-Selinger, W. Jacob, and A. von Keudell (unpublished).

<sup>14</sup> D. Boutard, W. Möller, and B. M. U. Scherzer, *Phys. Rev. B* **38**, 2988 (1988).

<sup>15</sup> D. Boutard, B. M. U. Scherzer, and W. Möller, *J. Appl. Phys.* **65**, 3833 (1989).

<sup>16</sup> R. W. Collins, *Rev. Sci. Instrum.* **60**, 3212 (1989).

<sup>17</sup> A. von Keudell and W. Jacob, *J. Appl. Phys.* **79**, 1092 (1996).

<sup>18</sup> T. Schwarz-Selinger, A. von Keudell, and W. Jacob, *J. Appl. Phys.* **86**, 1 (1999).